A Gallium–Nitride Push–Pull Microwave Power Amplifier

Jong-Wook Lee, Lester F. Eastman, *Life Fellow, IEEE,* and Kevin J. Webb, *Senior Member, IEEE*

***Abstract*—A highly efficient linear, broad-band AlGaN–GaN high electron-mobility transistor (HEMT) push–pull microwave power amplifier has been achieved using discrete devices. Instrumental was a low-loss planar three-coupled-line balun with integrated biasing. Using two 1.5-mm GaN HEMTs, a push–pull amplifier yielded 42% power-added efficiency with 28.5-dBm input power at 5.2 GHz, and a 3-dB bandwidth of 4–8.5 GHz was achieved with class-B bias. The output power at 3-dB gain compression was 36 dBm under continuous-wave operation. Along with the high efficiency, good linearity was obtained compared to single-ended operation. The second harmonic content of the amplifier was more than 30 dB down over the 4–8.5-GHz band, and a two-tone excitation measurement gave an input third-order intercept point of 31.5 dBm at 8 GHz. These experimental results and an analysis of the periodic load presented by the output balun suggest the plausibility of broad-band push–pull operation for microwave systems with frequency diversity.**

***Index Terms*—Balun, broad-band amplifier, gallium nitride, high electron-mobility transistor (HEMT), push–pull, silicon carbide.**

I. Introduction

WIDE-BANDGAP GaN (3.4 eV) offers a higher breakdown field ($\geq$3 MV/cm) and relatively lower intrinsic carrier generation than smaller bandgap semiconductors such as GaAs and Si [1]. With these characteristics, AlGaN–GaN high electron-mobility transistors (HEMTs) can operate under high drain voltage and high temperature. The current drive capability of GaN HEMTs is also good due to the very high sheet carrier density (1×10^{13}/cm^2) and high saturation velocity (1.2×10^7 cm/s) [2]. When high thermal conductivity (3.3 W/cm $\cdot$ K) semi-insulating SiC substrates are used, the low thermal impedance path provides high power density operation. These transport properties and power-handling capabilities lead to the promise of GaN HEMTs for high-power high-temperature microwave applications. Operation of GaN HEMTs has been demonstrated up to K-band [3], and a continuous-wave (CW) power density of 10.7 W/mm at 10 GHz [4] and a pulsed power of 113 W at 1.95 GHz [5] have been reported.

Manuscript received December 20, 2002; revised June 27, 2003. This work was supported by the Office of Naval Research (ONR) under Contract N00014-98-1-0371 and Contract N00014-99-C-0172. The discrete GaN devices were fabricated under ONR Contract N00014-99-C-0172.

J.-W. Lee was with the School of Electrical and Computer Engineering, Purdue University, West Lafayette, IN 47907 USA. He is now with the Department of Electrical and Computer Engineering, University of Illinois at Urbana-Champaign, Urbana, IL 61801 USA.

L. F. Eastman is with the School of Electrical and Computer Engineering, Cornell University, Ithaca, NY 14853 USA.

K. J. Webb is with the School of Electrical and Computer Engineering, Purdue Univesity, West Lafayette, IN 47907 USA (e-mail: webb@purdue.edu).

Digital Object Identifier 10.1109/TMTT.2003.818936

Recent applications of GaN HEMTs in broad-band power amplifiers have included a monolithic nonuniform distributed amplifier with a cascode-connected gain cell [6], an amplifier with distributed input, and corporate output combining that employed flip-chip bonded devices [7], an amplifier with *LCR* matching having an input power splitter and an output combiner [8], and a two-stage reactively matched monolithic-microwave integrated-circuit (MMIC) amplifier with backside via-holes through the SiC substrate [9]. While these GaN-based amplifiers have achieved high power performance, the results have been achieved at the expense of either linearity or power-added efficiency (PAE). These amplifier designs have been based either on linear class-A operation, with the consequential limitation on efficiency, or nonlinear class-AB operation.

Class-B operation offers high PAE, thus relieving thermal dissipation problems. Linear operation can be achieved with a class-B push–pull implementation. Push–pull operation also provides a larger impedance transformation ratio than parallel in-phase combining, which is particularly important for large periphery devices. Push–pull operation with identical devices requires transformer-coupled excitation and transformer combining in order to achieve the necessary 180° phase shift. At microwave frequencies, this can be achieved using a balun (balanced to unbalanced transformer, from antenna nomenclature), such as the broad-band compensated balun proposed by Marchand [10]. Broad-band baluns can have octave bandwidths, and the impact on push–pull amplifier performance will be a function of this bandwidth and the out-of-band impedance. More precisely, the impedance as a function of frequency of the output balun, as seen by the devices, will have a significant impact on amplifier performance. Also, while GaN HEMTs are still in the development stage, the significant power densities achieved thus far suggest that the technology is ready for more efficient amplifier development. These issues are addressed in the context of realizing broad-band linear GaN power amplifiers.

Class-B push–pull amplifiers have been manufactured at microwave frequencies. An AlGaAs–GaAs amplifier for L/S-band was designed for cellular base-station applications, where an output power of 112 W and a PAE of 46% were achieved [11]. In an amplifier with four devices, two push and two pull, an output power of 0.46 W and a PAE of 25% at K/Ka-band were obtained [12]. Both these amplifiers used forms of the Marchand balun, but did not focus on the large-signal frequency-dependent characteristics associated with the use of these baluns. A previously developed W-band amplifier employing AlGaAs–InGaAs–GaAs HEMTs used a Lange coupler with an additional line length to realize narrow-band baluns [13]. The impact of the frequency-dependent impedance transformation of the output balun is addressed in this paper.

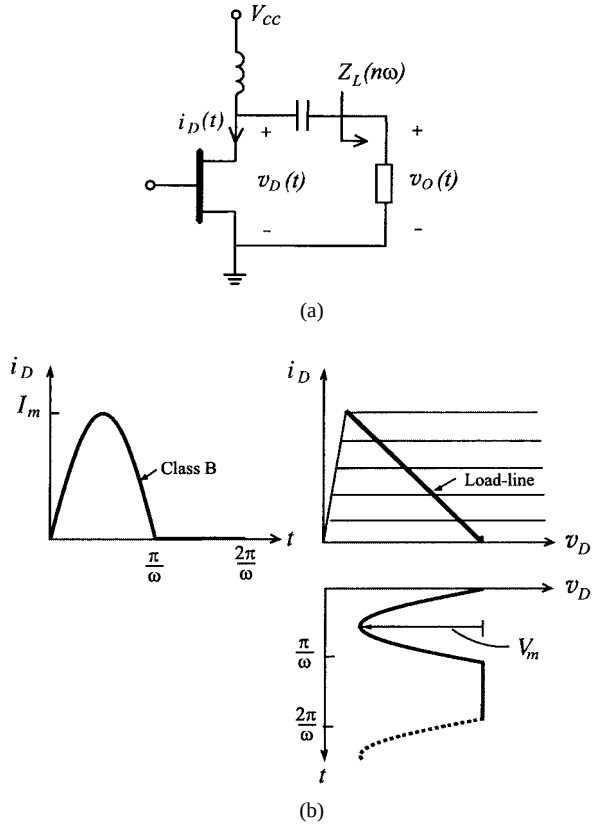

Fig. 1. (a) Schematic of the single-ended class-B amplifier with load $Z_L(n\omega)$. (b) Drain current/voltage waveform and load line for resistively terminated class-B operation.

Ideal class-B operation is described in Section II in order to provide a reference for measured efficiencies. The design and fabrication of planar broad-band baluns used in the push–pull amplifiers is presented in Section III. Section IV gives the amplifier design and measured results for the push–pull GaN amplifier using discrete HEMTs.

II. Class-B Operation

The impact of the frequency-dependent driving point impedance of the output balun on PAE is investigated in class-B operation, and various factors that influence efficiency and linearity are examined.

A single-ended class-B amplifier with a tuned circuit load is shown in Fig. 1(a), and the corresponding drain current and voltage waveforms with the assumption of a resistive load line is shown in Fig. 1(b). The dc drain bias point is $V_{\rm cc}$. The periodic half sinusoid $i_D(t)$ in Fig. 1(b) can be expressed as a Fourier series, giving

$$i_D(t) = \sum_{n=-\infty}^{\infty} I_D(n\omega)e^{jn\omega t} = \frac{I_m}{\pi} + \frac{I_m}{2}\sin(\omega t) - \frac{2I_m}{\pi}\sum_{n\geq 2,\text{even}}^{\infty}\frac{\cos(n\omega t)}{n^2-1} \quad (1)$$

where $I_D(n\omega)$ is the peak amplitude of the nth harmonic of the drain current. Assuming a real and constant load impedance for all harmonics ($Z_L(n\omega) = R_L$), the case in Fig. 1(b), the drain voltage Fourier expansion is

$$v_D(t) = V_{\rm cc} - \frac{V_m}{2}\sin(\omega t) + \frac{2V_m}{\pi}\sum_{n\geq 2,\text{even}}^{\infty}\frac{\cos(n\omega t)}{n^2-1} \quad (2)$$

where V_m is the maximum instantaneous drain voltage deviation from $V_{\rm cc}$. With a frequency-dependent load impedance $Z_L(n\omega), V_D(n\omega) = I_D(n\omega)Z_L(n\omega)$. The fundamental and harmonic component of the drain voltage will then depend on the driving point impedance of the output balun $Z_L(n\omega)$.

Consider now the class-B push–pull amplifier and the ideal case of a center-tapped input transformer providing the correct 180° phase-shifted gate voltage and an infinite bandwidth output transformer for each device having unity turns ratio. The output current obtained by combining two antiphase drain currents and using (1) shows that the push–pull amplifier is linear with an ideal linear device. Since HEMT characteristics are usually close to linear above threshold, low distortion operation is feasible for push–pull class-B power amplifiers with GaN HEMTs. For a linear push–pull amplifier, $P_{\rm out} = I_m^2 R_L/2 = V_m I_m/2$. The power supplied by both sources is $P_{\rm sup} = 2V_{\rm cc}I_m/\pi$ and, assuming full swing, $V_{\rm cc} = V_m$ and, therefore, the drain efficiency is $\pi/4$. Thus, the advantage of a push–pull amplifier is high efficiency and its linear transfer function.

The device knee voltage will limit achievable drain efficiency. For physical devices that dissipate gate power, PAE is also an important parameter, where $\text{PAE} = (P_{\rm out} - P_{\rm in})/P_{\rm sup}$. With $Z_L(n\omega)$ a function of frequency, linearity will be compromised.

Implementing a microwave push–pull amplifier requires either very small lumped-element transformers or some form of distributed transformer. The latter approach is described in this paper. The physical balun has finite bandwidth, nonzero insertion loss, imperfect magnitude and phase balance, and provides a frequency-dependent transformation of the load resistance. All of these factors can potentially serve to reduce the efficiency and detract from the linearity. However, the resonant balun offers favorable features when used as the output transformer in a push–pull amplifier.

III. Low-Loss Planar Three-Coupled-Line Balun

A low insertion-loss broad-band microstrip Marchand balun is shown in Fig. 2(a). The planar three-conductor balun with the outer resonators connected allows tight coupling to be achieved with relaxed inter-line spacing. The symmetric three-coupled-line balun can be analyzed by considering its correlation with the ideal coaxial balun of Fig. 2(b), [10]. Only two modes propagate in the system of Fig. 2(a), due to the presence of air bridges between the two outer conductors. The center conductor forms an open-terminated line, described by a mode similar to that in a coplanar waveguide (CPW), and the outer conductors form shorted resonators. These effectively combine to give a series open-circuit stub and shunt short-circuit stub, as in Fig. 2(b). The line lengths (L_a, L_b, L_{ab}) in Fig. 2(b) are all one quarter-wavelength at the center frequency. Since the two contributing microstrip modes have different phase constants, the microstrip resonator lengths will differ. In this case, some effective length can be used.

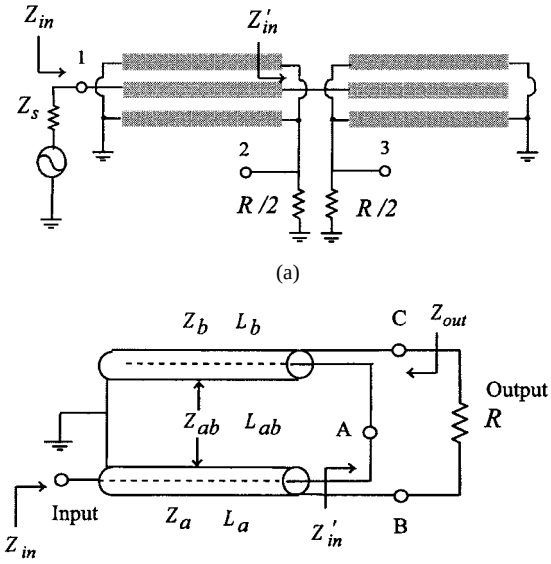

Fig. 2. (a) Microstrip balun implementation using three coupled lines. $Z_s = 50\,\Omega, R = 50\,\Omega$. (b) Coaxial balun schematic. The line lengths are one quarter-wavelength at the center frequency f_0.

The characteristic impedances of the balun were obtained from an analysis based on bandwidth and input/output impedance under the TEM assumption. The coupled-line dimensions corresponding to the desired characteristic impedances were obtained using a two-dimensional (2-D) quasi-TEM balun model [14]. The final design validation was evaluated using Agilent Momentum,[1] a full-wave electromagnetic simulator. For high (bias) current, an appropriately large conductor cross section was needed. To achieve wide lines, a 375-μm-thick high thermal conductivity AlN substrate ($\epsilon_r = 8.5$) was used. The linewidths were all 80 μm, with 20-μm spacing, and the resonator lengths were 3900 μm ($f_0 = 8$ GHz). The impedance transformation is from 50 Ω unbalanced to 50 Ω balanced, which is 25 Ω to ground, i.e., each device gate and drain needs to be matched to 25 Ω at the center frequency. This lower impedance eases the matching to large periphery devices. The measured back-to-back balun performance for two cascaded baluns is shown in Fig. 3. The insertion loss is less than 0.5 dB per balun over 5–9.5 GHz. The measured amplitude imbalance was less than 1 dB, and the phase imbalance was $\pm 10^\circ$, over 5–11 GHz [14].

For the coaxial Marchand balun circuit shown in Fig. 2(b), assuming equal line lengths ($L_a = L_b = L_{ab}$), the impedance transformation of the coaxial balun will be periodic in frequency, with period $2f_0$. To see the load impedance for a push–pull device, consider the impedance at nodes C–B, $Z_{\text{out}} = R_{\text{out}} + jX_{\text{out}}$, i.e., from the balanced end, which is

$$R_{\text{out}} = \frac{Z_a Z_{ab}^2}{Z_a^2 \cot^2\theta + (Z_{ab} - Z_b \cot^2\theta)^2} \tag{3}$$

$$X_{\text{out}} = \frac{Z_a^2 Z_{ab} \cot\theta - Z_b Z_{ab} \cot\theta (Z_{ab} - Z_b \cot^2\theta)}{Z_a^2 \cot^2\theta + (Z_{ab} - Z_b \cot^2\theta)^2} \tag{4}$$

[1]*Agilent Advanced Design System (ADS)*, Agilent Technol., Palo Alto, CA, 2000.

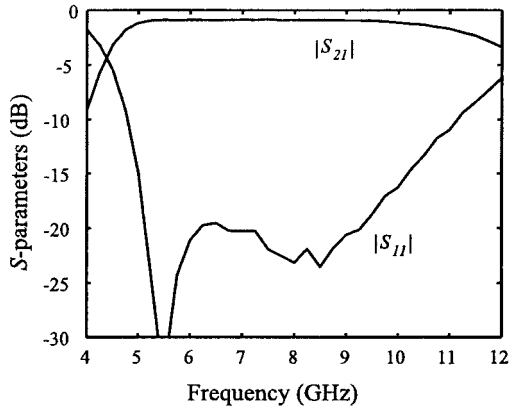

Fig. 3. Measured back-to-back balun response of the two cascaded baluns.

with $\theta = ((\pi/2)(f/f_0))$ and f_0 the band center frequency where the electrical length equals one quarter-wavelength.

From the impedance expressions of (3) and (4), it is evident that the same impedance is presented, i.e., a passband occurs, at odd multiples of $f_0(f_0, 3f_0, \ldots)$. Along with the periodic impedance transformation property, the output balun provides a short-circuit termination for even harmonics. If $Z_a = R$, then from (3), $R_{\text{out}} = R$ when $\theta = (2n+1)\pi/2, n = 0, 1, 2, \ldots$, i.e., at $f_0, 3f_0, \ldots$, and $X_{\text{out}} = 0$. At $\theta = n\pi$ or $2f_0, 4f_0, \ldots, R_{\text{out}} = 0$ and $X_{\text{out}} = 0$. This result is significant for push–pull combining. It suggests that for frequencies near f_0, the even harmonics that appear in a passband will be approximately eliminated by those from the other device, as in the ideal transformer. Also, those harmonics appearing in a stopband will have small contribution to the drain voltage and can be expected to have small contribution to the output power spectrum. For frequencies that deviate appreciably from f_0, some nonlinearity may occur. Therefore, over some band of frequencies near f_0, the linearity and efficiency could be expected to be similar to that of the ideal infinite bandwidth transformer. This suggests that a moderately broad-band push–pull amplifier should be feasible with a finite bandwidth balun due to its periodic impedance transformation property.

The frequency response of the microstrip balun shown in Fig. 2(a) was studied using an Agilent *ADS* transmission-line model. The output port impedance of the microstrip balun Z_{out} is the load seen by the drains of the push–pull pair. The simulation for Z_{out} for the $f_0 = 8$ GHz balun is given in Fig. 4. As expected, the balun approximately provides a short-circuit termination for the second harmonic $(2f_0)$. The real part of Z_{out} is very small over a significant bandwidth about $2f_0$, and the reactance is small and has an approximately linear dependence on frequency. Depending on balun design, there will be a transition region between passband and stopband where the degree of harmonic termination will vary with frequency, and where the linearity will be worse. Fig. 4 indicates that this balun should be effective in a push–pull amplifier operated over most of the 4–10-GHz range, except for small bands around 6 and 10 GHz. However, the amplifier results that will be presented indicate that harmonic suppression is excellent over the entire band.

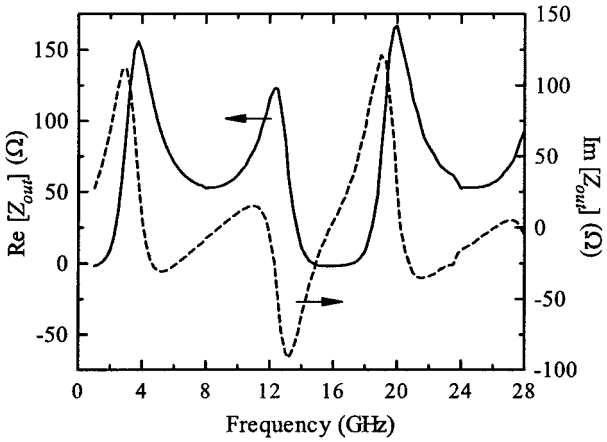

Fig. 4. Calculated balanced output port impedance of the microstrip balun versus frequency. The balun center frequency f_0 is 8 GHz.

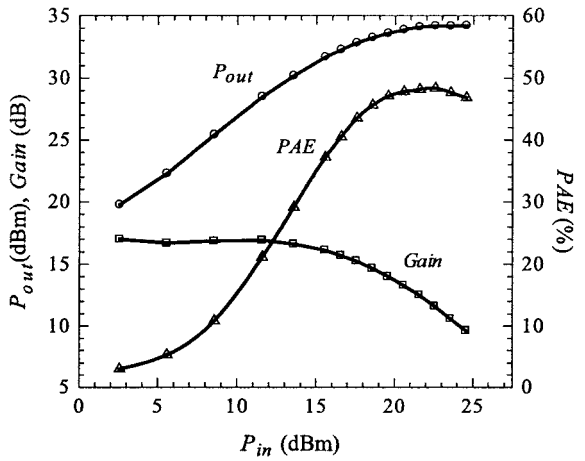

Fig. 5. Measured CW power sweep of 1.5-mm AlGaN–GaN HEMT on SiC at 4 GHz with $V_{\rm ds} = 18$ V, $V_{\rm gs} = -2.47$ V using input/output tuners.

IV. GaN Class-B Push–Pull Amplifier

A. Gallium–Nitride HEMT Device Technology

The fabrication, dc, and RF testing results for the discrete GaN HEMTs used in study have been reported previously [15]. The AlGaN–GaN HEMT layer structure was grown by metal organic chemical vapor deposition (MOCVD) on a semi-insulating 4H-SiC substrate. The push–pull amplifier presented in this paper used 1.5-mm periphery devices ($12 \times 125\ \mu$m) having 0.35-μm gate lengths and source ground via-holes connected with air bridges. These devices had a maximum of approximately 600-mA/mm drain current, an f_T of 25 GHz, and an $f_{\max}$ of 43 GHz, and the pinchoff voltage was -3 V. Typical three-terminal gate–drain breakdown voltages ranged between 60–70 V. A CW power sweep yielded a PAE of over 48% with a saturated gain of 12.5 dB at 4 GHz when biased at $V_{\rm ds} = 18$ V, $V_{\rm gs} = -2.47$ V, and using input/output tuners, as shown in Fig. 5.

B. Circuit Design and Fabrication

A modified Curtice cubic model with temperature-dependent drain current modeling coefficients [16] was used as a user-defined model for the GaN HEMTs in Agilent *ADS*. As conventional methods based on fitting the dc *I–V* curve are not a valid indicator of the measured power spectrum, due to RF dispersion and thermal heating [17], [4], a pulsed *I–V* measurement was used to characterize the devices and construct the nonlinear model. Temperature-dependent drain current coefficients and bias-dependent model parameters were extracted from dc and pulsed *I–V* characteristics measured at different temperatures and S-parameters measured at 80 different bias points. The model was validated using measured power sweep data with class-B bias. This large-signal model was used to examine the bias-dependent small-signal stability and the bias-dependent amplifier performance.

The optimum load impedance for the 1.5-mm device was determined using a focus load-pull system tuned for efficiency at class-B bias. Higher efficiency could be achieved at a relatively lower drain bias so a drain bias of 15 V was chosen. The optimum load reflection coefficient $(\Gamma_{L,\rm opt})$ was measured to be $0.572\ \angle 102.2°$ at 5 GHz. The frequency-dependent balun input impedance $Z_{\rm in}$ and the balanced output impedance $Z_{\rm out}$ were obtained using an Agilent *ADS* transmission-line model. The output matching network transforms $Z_{\rm out}/2$ to the optimum load impedance $Z_{L,\rm opt}(=25(1+\Gamma_{L,\rm opt})/(1-\Gamma_{L,\rm opt}))$ at 5 GHz. An open-circuit stub match was designed for this purpose. With the determined output matching network in place, the input matching network was designed to transform the device input impedance (found from $\Gamma_{D,\rm in} = S_{11} + (S_{12}S_{21}\Gamma_{L,\rm opt})/(1 - S_{22}\Gamma_{L,\rm opt})$, where S_{ij} are the device S-parameters) to 25 Ω. Considering the lower available gain at higher frequencies, the input matching network was designed to match at 8 GHz for gain flatness. The same matching network was used in the balanced lines for both device inputs, and likewise for the outputs, thereby maintaining symmetry.

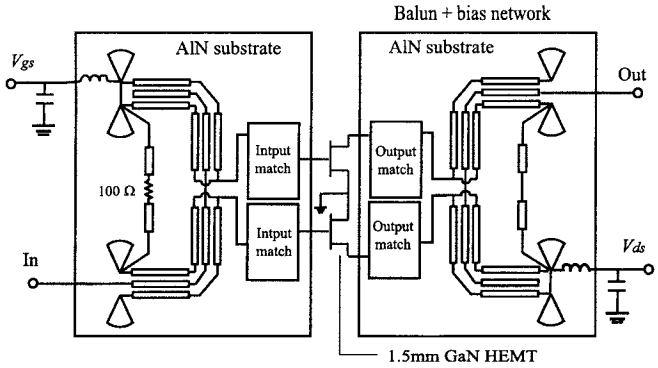

Fig. 6. Schematic of the push–pull amplifier with the balun and biasing scheme.

Fig. 6 shows a schematic of the push–pull amplifier with the balun that incorporates the dc-biasing scheme. The bias is injected through a radial stub, which also acts as the balun resonator RF ground. This scheme takes advantage of the dc isolation provided by the coupled-line structure and, thus, eliminates the need for RF-dc decoupling capacitors. Using the high-impedance line between RF ground points provided by the radial stubs, the dc bias is supplied to both active devices with a single bias injection point for the gate and drain. For stability, a 100-Ω TiW resistor was included in the center of the high-impedance shunt connection line of the input balun, and a 100-pF chip capacitor was used for additional RF bypassing in both the input and output baluns.

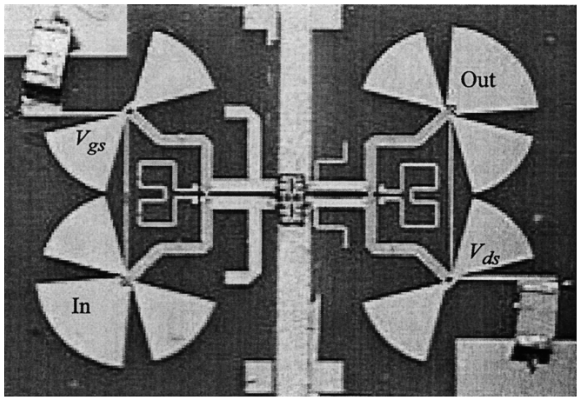

Fig. 7. Photograph of the fabricated push–pull amplifier with discrete GaN HEMTs, showing the matching stubs, dc-bias network, chip capacitors, and the input/output baluns with radial stub grounding. Each substrate containing a balun and matching network is approximately 0.5 in × 0.4 in.

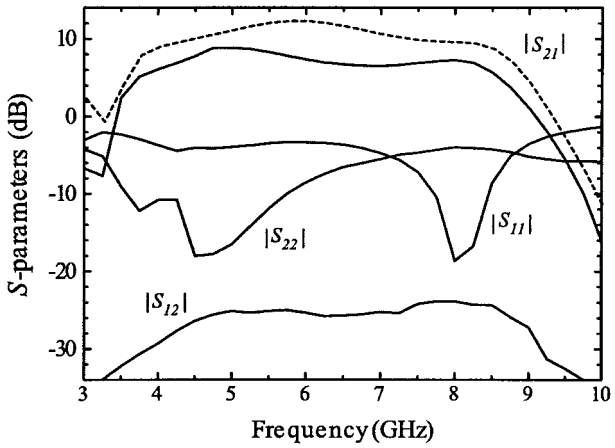

Fig. 8. Measured small-signal S-parameters for the push–pull amplifier. $V_{\rm ds} = 15$ V and $V_{\rm gs} = -2.4$ V. The dashed line is the simulated $|S_{21}|$.

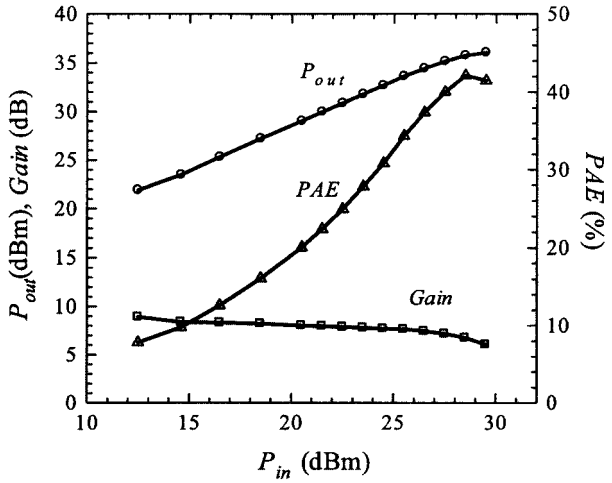

Fig. 9. Measured power sweep at 5.2 GHz in class-B push–pull mode in a 50-Ω system. $V_{\rm ds} = 15$ V and $V_{\rm gs} = -2.5$ V.

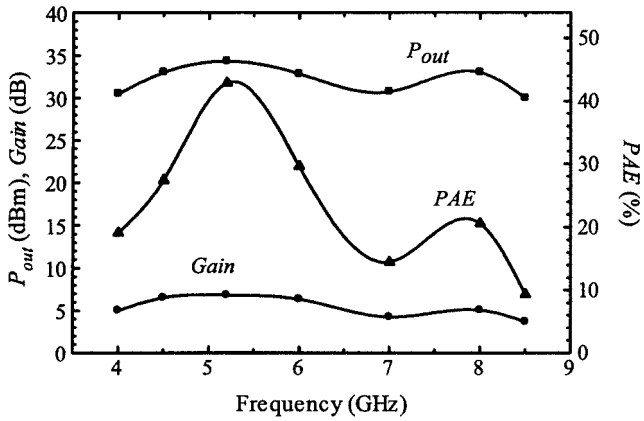

Fig. 10. Measured output power, saturated gain, and PAE versus frequency for the push–pull amplifier at approximately the 2-dB gain compression point. $V_{\rm ds} = 12$ V and $V_{\rm gs} = -2.5$ V.

The fabricated amplifier is shown in Fig. 7. The balun and input/output matching networks were fabricated on the AlN substrate, metallized with 2.5-μm-thick gold. The 1.5-mm GaN HEMTs were attached to a gold-plated brass fixture using a high thermal conducting epoxy (DIEMAT 6030Hk), which had a thermal conductivity of 60 W/m · K and 6 $\mu\Omega$ · cm resistivity, and a 1-mil Au bond wire was used for device-to-balun connection. Additional radial stubs at the input and output provide top-side RF grounding for on-wafer probing. Each substrate, containing a balun and matching network, is approximately 0.5 in × 0.4 in.

C. Measured Results

The small-signal S-parameter results for the push–pull amplifier at $V_{\rm ds} = 15$ V and $V_{\rm gs} = -2.4$ V are shown in Fig. 8. The gain at 5 GHz is approximately 9 dB and the 3-dB bandwidth is 4–8.5 GHz. The measured $|S_{22}|$ at 5 GHz is -16 dB and $|S_{11}|$ is -18 dB at 8 GHz. Fig. 9 shows the CW output power sweep at 5.2 GHz with the amplifier biased at $V_{\rm ds} = 15$ V and $V_{\rm gs} = -2.5$ V. The bias current was 117 mA at small input drive, and gradually increased to 0.5 A. With 28.5 dBm of input power, a PAE of 42% and a CW power of 35.5 dBm were measured. This PAE is the highest achieved for a linear GaN power amplifier to date. Fig. 10 shows the output power, gain, and PAE measured at approximately the 2-dB gain compression point at each frequency, using a bias of $V_{\rm ds} = 12$ V and $V_{\rm gs} = -2.5$ V. The PAE ranged from 42% to 14% over 4–8 GHz. The drop in PAE at higher frequency is due to the mismatch to the optimum load impedance and reduced device gain.

To assess the linearity of the push–pull amplifier, single tone harmonic content and two-tone intermodulation measurements were performed. A single-ended class-B amplifier with matching was fabricated using a 1.5-mm device, and the second harmonic level was measured under the same bias condition. Fig. 11 shows the measured fundamental output power and second harmonic levels for the push–pull amplifier biased at $V_{\rm ds} = 15$ V and $V_{\rm gs} = -2.6$ V, as well as that for the single-ended amplifier. The second harmonic levels measured with 20-dBm input power level were well below -30 dBc over the 4–8.5-GHz range for the push–pull amplifier, and were better than the single-ended amplifier over virtually all of the frequency range measured. As the measurement shows, the level of harmonic suppression is frequency dependent, and is influenced by the nonlinearity of the device, the nonideal balance characteristics, and the frequency-dependent load impedance presented by the output balun.

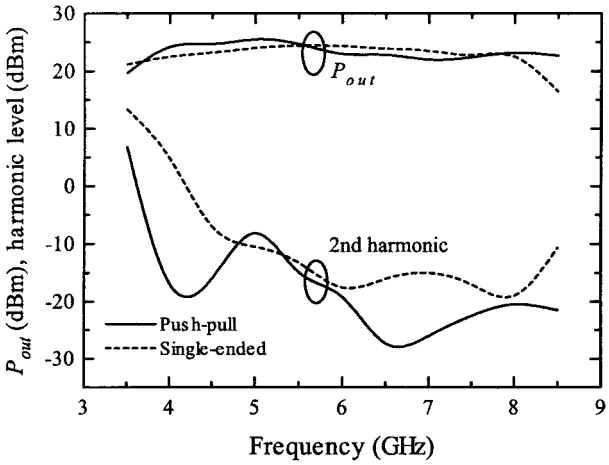

Fig. 11. Measured output power and second harmonic levels for the single-ended and push–pull amplifier versus frequency with 20-dBm input power. $V_{\rm ds} = 15$ V and $V_{\rm gs} = -2.6$ V.

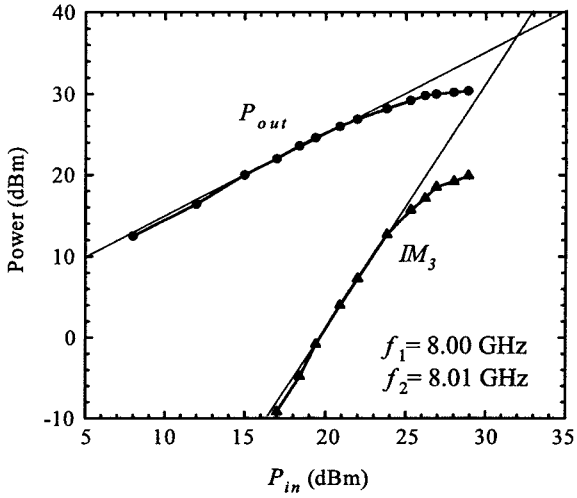

Fig. 12. Measured two-tone intermodulation ($f_1 = 8.00$ GHz, $f_2 = 8.01$ GHz) response of the push–pull amplifier at 8 GHz versus input power. $V_{\rm ds} = 12$ V and $V_{\rm gs} = -2.6$ V.

Fig. 12 shows the measured two-tone intermodulation performance of the push–pull amplifier versus input power with $V_{\rm ds} = 12$ V and $V_{\rm gs} = -2.6$ V at 8 GHz. A low drain bias, where good PAE was obtained, was chosen. Using the extrapolated 1 : 1 slope of the fundamental output power and the 3 : 1 slope of the third-order intermodulation product (IM_3), an input third-order intercept point (IIP_3) of 31.5 dBm is obtained [18]. The output third-order intercept point (OIP_3) is 37.5 dBm, and the two-tone 1-dB output power $P_{1\,\mathrm{dB,2tone}}$ obtained at $P_{\rm in} = 25$ dBm is 29 dBm, resulting in $\mathrm{OIP}_3 - P_{1\,\mathrm{dB,2tone}} = 8.5$ dB. For comparison, a GaN lossy match amplifier [6] operated at class-A bias gave 7.8 dB at 6 GHz. The push–pull amplifier has a higher input third-order intercept point than this class-A amplifier. The intermodulation characteristic of the amplifier is expected to improve at higher drain bias because the high drain-bias voltage possible in a wide-bandgap GaN HEMT permits more linear transfer characteristics, i.e., smaller changes in nonlinear device parameters during large-signal operation for the same output power [19], [20].

V. Conclusion

A GaN-based push–pull linear microwave power amplifier has been presented. Push–pull operation was achieved using a symmetric three-coupled-line balun that was designed to provide good output balance characteristics, simple dc biasing for the amplifier, and especially low insertion loss. The periodic load presented by the output balun provides either correct cancellation, in the case of odd multiples of the passband center frequency, or a low-impedance termination at even multiples. Fortuitously, this means that broad-band resonant baluns can be used to achieve good broad-band push–pull amplifiers over a significant bandwidth. The discrete GaN HEMT push–pull amplifier, therefore, produced excellent linearity and quite high efficiency. Multiple devices, in the form of broad-band amplifiers, can also be combined as push–pull pairs. With improvements in device technology, the efficiency, power, and linearity of GaN amplifiers will increase.

Acknowledgment

The authors thank S. Sheppard, Cree Inc., Durham, NC, for providing the discrete GaN devices. The authors gratefully acknowledge Y.-F. Wu of Cree Lighting, Goleta, CA, for discussions.

References

[1] I. Daumiller, C. Kirchner, M. Kamp, K. J. Ebeling, and E. Kohn, "Evaluation of the temperature stability of AlGaN/GaN heterostructure FET's," *IEEE Electron Device Lett.*, vol. 20, pp. 448–450, Sept. 1999.

[2] L. F. Eastman, V. Tilak, J. Smart, B. M. Green, E. M. Chumbes, R. Dimitrov, H. Kim, O. S. Ambacher, N. Weimann, T. Prunty, M. Murphy, W. J. Schaff, and J. R. Shealy, "Undoped AlGaN/GaN HEMTs for microwave power amplification," *IEEE Trans. Electron Devices*, vol. 48, pp. 479–485, Mar. 2001.

[3] M. Micovic, J. S. Moon, A. Kurdoghlian, P. Hashimoto, D. Wong, L. McCray, T. Hussain, and P. Janke, "K-band GaN power HFET's with 6.6 W/mm CW saturated output power density and 35% power added efficiency at 20 GHz," in *Device Res. Conf. Dig.*, Notre Dame, IN, June 2001, pp. 199–200.

[4] V. Tilak, B. Green, H. Kim, T. Prunty, J. Smart, J. Shealy, and L. F. Eastman, "Influence of barrier thickness on the high-power performance of AlGaN/GaN HEMTs," *IEEE Electron Device Lett.*, vol. 22, pp. 504–506, Nov. 2001.

[5] Y. Ando, Y. Okamoto, H. Miyamoto, N. Hayama, T. Nakayama, K. Kasahara, and M. Kuzuhara, "A 110-W AlGaN/GaN heterojunction FET on thinned sapphire substrate," in *Int. Electron Devices Meeting Tech. Dig.*, Washington, DC, Dec. 2001, pp. 381–384.

[6] B. M. Green, V. Tilak, S. Lee, H. Kim, J. A. Smart, K. J. Webb, J. R. Shealy, and L. F. Eastman, "High-power broad-band AlGaN/GaN HEMT MMICs on SiC substrates," *IEEE Trans. Microwave Theory Tech.*, vol. 49, pp. 2486–2493, Dec. 2001.

[7] J. J. Xu, Y.-F. Wu, S. Keller, G. Parish, S. Heikman, B. J. Thibeault, U. K. Mishra, and R. A. York, "1–8 GHz GaN-based power amplifier using flip-chip bonding," *IEEE Microwave Guided Wave Lett.*, vol. 7, pp. 277–279, July 1999.

[8] J. J. Xu, Y.-F. Wu, S. Keller, G. Parish, S. Heikman, U. K. Mishra, and R. A. York, "A 3–10 GHz *LCR*-matched power amplifier using flip-chip mounted AlGaN/GaN HEMTs," in *IEEE MTT-S Int. Microwave Symp. Dig.*, vol. 2, 2000, pp. 959–962.

[9] J. W. Palmour, S. T. Sheppard, R. P. Smith, S. T. Allen, W. L. Pribble, T. J. Smith, Z. Ring, J. J. Sumakeris, A. W. Saxler, and J. W. Milligan, "Wide bandgap semiconductor devices and MMIC's for RF power applications," in *Int. Electron Devices Meeting Tech. Dig.*, Washington, DC, Dec. 2001, pp. 385–388.

[10] N. Marchand, "Transmission-line conversion transformer," *Electronics*, vol. 17, no. 12, pp. 142–145, Dec. 1944.

[11] I. Takenaka, K. Ishikura, H. Takahashi, K. Asno, J. Morikawa, K. Satou, K. Kishi, K. Hasegawa, K. Tokunaga, F. Emori, and M. Kuzuhara, "L/S-band 140-W push–pull power AlGaAs/GaAs HFET's for digital cellular base stations," *IEEE J. Solid-State Circuits*, vol. 34, pp. 1181–1186, Sept. 1999.

[12] J. Schellenberg and H. Do-ky, "A push–pull power MMIC operating at K/Ka-band frequencies," in *IEEE MTT-S Int. Microwave Symp. Dig.*, 1999, pp. 971–974.

[13] H. Wang, R. Lai, M. Beidenbender, G. S. Dow, and B. R. Allen, "Novel W-band monolithic push–pull power amplifiers," *IEEE J. Solid-State Circuits*, vol. 30, pp. 1055–1061, Oct. 1995.

[14] J.-W. Lee and K. J. Webb, "Analysis and design of low-loss planar microwave baluns having three symmetric coupled lines," in *IEEE MTT-S Int. Microwave Symp. Dig.*, vol. 1, Seattle, WA, June 2002, pp. 117–120.

[15] S. T. Sheppard, K. Doverspike, W. L. Pribble, S. T. Allen, J. W. Palmour, L. T. Kehias, and T. J. Jenkins, "High-power microwave GaN/AlGaN HEMT's on semi-insulating silicon carbide substrates," *IEEE Electron Device Lett.*, vol. 20, pp. 161–163, Apr. 1999.

[16] J.-W. Lee, S. Lee, and K. J. Webb, "Scalable large-signal device model for high power-density AlGaN/GaN HEMT's on SiC," in *IEEE MTT-S Int. Microwave Symp. Dig.*, vol. 2, May 2001, pp. 679–682.

[17] E. Kohn, I. Daumiller, P. Schmid, N. X. Nguyen, and C. N. Nguyen, "Large signal frequency dispersion of AlGaN/GaN heterostructure field effect transistors," *Electron. Lett.*, vol. 35, no. 12, pp. 1022–1024, June 1999.

[18] S. C. Cripps, *RF Power Amplifiers for Wireless Communications*. Norwood, MA: Artech House, 1999.

[19] N. Vellas, C. Gaquiere, Y. Guhel, M. Werquin, F. Bue, R. Aubry, S. Delage, F. Semond, and J. C. De Jaeger, "High linearity performances of GaN HEMT devices on silicon substrate at 4 GHz," *IEEE Electron Device Lett.*, vol. 23, pp. 461–463, Aug. 2002.

[20] M. Nagahara, T. Kikkawa, N. Adachi, Y. Tateno, S. Kato, M. Yokoyama, S. Yokogawa, T. Kimura, Y. Yamaguchi, N. Hara, and K. Joshin, "Improved intermodulation distortion profile of A1GaN/GaN HEMT at high drain bias voltage," in *Int. Electron Devices Meeting Tech. Dig.*, 2002, pp. 693–696.

Jong-Wook Lee was born on April 6, 1970, in Korea. He received the B.S. and M.S. degrees in electrical engineering from the Seoul National University, Seoul, Korea, in 1993 and 1997, respectively.

From 1994 to 1996, he served in the military. From 1998 to 2002, he was a Research Assistant with the School of Electrical and Computer Engineering, Purdue University, West Lafayette, IN. In 2001, he served as a president of Purdue University Electrical Engineering Korean Association. Since 2003, he has been a Post-Doctoral Research Associate with the University of Illinois at Urbana-Champaign. His research interests are in the area of microwave/RF device characterization, modeling, and circuit design.

Mr. Lee was the recipient of the 1997 Korean Government Overseas Scholarship.

Lester F. Eastman (A'53–M'58–SM'65–F'69–LF'94) is currently the John L. Given Foundation Chair Professor of Engineering at Cornell University, Ithaca, NY. Beginning in 1998, he became devoted full time to graduate research and currently has nine graduate students under his supervision. In 1957, he joined the faculty of electrical engineering at Cornell University. He also serves as a member of the graduate fields of applied physics and materials science. Since 1965, he has conducted research on compound semiconductor materials and high-speed devices and circuits, and has been active in organizing workshops and conferences on these subjects elsewhere since 1965 and at Cornell University since 1967. In 1977, he joined other Cornell University faculty members in obtaining funding and founding the National Research and Resource Facility for Submicron Structures at Cornell (now Cornell Nanofabrication Facility). Also in 1977, he founded the Joint Services Electronics Program and directed it until 1987. He has supervised 111 Ph.D. dissertations, 41 M.S. theses, and 81 post-doctoral studies. In his research group, effort is underway on molecular beam epitaxy, microwave transistors, high-speed semiconductor lasers, and fundamental phenomena in compound semiconductor quantum electron and optical devices. From 1978 to 1979, he was on leave at the Massachusetts Institute of Technology (MIT) Lincoln Laboratory, and from 1985 to 1986, he was with the IBM Watson Research Laboratory. He has served as a consultant for several industries.

Dr. Eastman is a member of the National Academy of Engineering (since 1986) and was appointed the John L. Given Foundation Chair Professor of Engineering at Cornell University in January 1985. In 2001, he became a Fellow of the American Physical Society. During 1983, he was the IEEE Electron Device Society National Lecturer. He was a member of the U.S. Government Advisory Group on Electron Devices from 1978 to 1988. From 1987 to 1993, he served as a member of the Kuratorium (Visiting Senior Advisory Board) of the Fraunhofer Applied Physics Institute, Freiburg, Germany. He was the recipient of the 1991 GaAs Symposium Award and the Heinrich Welker Medal for his "contributions to the development of ballistic electron devices, planar doping, buffer layers, and Al1nAs/GaInAs/InP heterostructures." He was also the recipient of the 1994 Alexander von Humboldt Senior Fellowship and the 1995 Aldert van der Ziel Award. He was the recipient of the 1999 IEEE Graduate Teaching Award, the 2000 IEEE Third Millennium Medal, and the 2002 J. J. Ebers Award of the IEEE Electron Device Society.

Kevin J. Webb (S'81–M'84–SM'98) received the B.Eng. and M.Eng. degrees from the Royal Melbourne Institute of Technology, Melbourne, Australia, in 1978 and 1983, respectively, the M.S.E.E. degree from the University of California at Santa Barbara, in 1981, and the Ph.D. degree from the University of Illinois at Urbana-Champaign, in 1984.

He is currently a Professor with the School of Electrical and Computer Engineering, Purdue University, West Lafayette, IN. During the 2003 calendar year, he is a Visiting Professor with the Massachusetts Institute of Technology (MIT), Cambridge.